ingegneria sismica
International Journal of Earthquake Engineering
Anno XLIII - Num. 1 - 2026

Research on the construction of early identification and early warning system for psychological crisis of adolescents' online social behavior based on multimodal data fusion computational analysis

Hui Xu[1], *Jiahao Wang*[1], *Huazhi Li*[2] *and Huanhuan Luo*[3,*]

[1] Student Affairs Department of the Party Committee, Tarim University, Alar, Xinjiang, 843300, China
[2] School of Media and Technology, Liaocheng University, Liaocheng, Shandong, 252000, China
[3] Medical College, Tarim University, Alar, Xinjiang, 843300, China

SUMMARY: *In this paper, electrocardiography, electroencephalography, oximetry, picoelectricity and body temperature will be selected as the analyzed signals, and the corresponding multimodal acquisition scheme and the overall design of the acquisition system will be proposed. Aiming at the problem that physiological signals are susceptible to external interference, the wavelet transform method is applied within the acquisition system to achieve the purpose of noise reduction processing of the acquired physiological signals. Comparing with the MP150 system to collect resting state data, the signals collected by this system and the MP150 system are basically similar in waveform amplitude, phase and spectral characteristics, which verifies the validity of the physiological signals collected by this system. In order to facilitate early diagnosis of psychological crises expressed in the form of the social behavior of adolescents through the Internet, an improved PSO algorithm is proposed in this study to fine-tune the parameter setting of the BP neural network, which will result in a psychological state identification model based on the improved PSO-BP neural network. The results show that the recognition accuracy reaches 95.5% compared with the actual test set classification. In this study, a mental health early warning system is designed, which is based on a multimodal acquisition system and uses the mental state recognition model to analyze physiological data, as a way to detect the psychological state of the adolescents being tested, and then make timely and accurate warnings.*

KEYWORDS: *wavelet transform; improved PSO-BP; mental state recognition; multimodal data acquisition system; mental health warning*

1 Introduction

With the development of the Internet, online socializing has become a new communication channel in human life [1]. It not only helps people get rid of the limitations of geographical location and time but also greatly reduces the cost of interpersonal communication while increasing the efficiency and convenience of communication, and this way of interpersonal communication has become the choice of the general public [2, 3], of which teenagers accounted for a large proportion, and online socialization has become an important form of interpersonal communication that should not be neglected by Chinese teenagers at the present

*luohuanhuan321@163.com
https://doi.org/10.65102/is2026500
Published: 30 April, 2026

time [4]. However, online social behaviors are filled with all kinds of cyberbullying, false information, and extreme emotions, which not only affect adolescents' academic performance, but also may trigger a series of psychological crises, such as loneliness, depression, and antisociality [5-7]. Therefore, it is of great theoretical value and practical significance to explore the identification of psychological crises and early warning measures for adolescents' online social behaviors.

Although the traditional text-based sentiment analysis method can reflect the psychological health status of adolescents to a certain extent, this kind of single-modal data analysis cannot fully grasp the dynamic and complex psychological state of adolescents [8, 9]. Since the psychological crisis of adolescents' online social behavior is interwoven with various factors, including language expression, social network, online time and so on, which leads to the traditional method can not meet the demand of comprehensive emotion identification and early warning, but this multifactor also provides the application conditions for multimodal data fusion computing. The term "multimodal data fusion computing" implies an area of technology that improves accuracy in processing information and making decisions with the use of heterogeneous data [10, 11]. With the help of multimodal data fusion computing analysis, building a psychological crisis early identification and warning system can be used as a way to organize various kinds of data obtained from adolescents' social online activities, such as verbal text, video, images, social networks, etc., and analyze and mine them with the help of deep learning and other intelligent tools [12-14]. Thus, it reveals the correlation between adolescents' psychological state and multi-source behavioral characteristics, and realizes the identification and early warning of psychological crisis, which is of great significance for safeguarding adolescents' mental health [15, 16].

Recently, research on the psychological dilemmas caused by adolescents' online social interactions has become significantly abundant within a number of relevant sub-disciplines. Literature [17] looked into the impact of online social interaction on adolescent psychological health, indicating that while online social behavior may result in beneficial results by promoting friendships, it may also have detrimental effects on adolescents due to deteriorating family relations. The significance of monitoring adolescents' online social behavior for their parents and teachers has been emphasized due to the findings of literature [17]. Literature [18] explored the association between adolescent mental health and online social engagement in relation to the time spent on social platforms, and possible associations with various psychological disorders like depression and low self-esteem, and pointing out the controversial nature of the current findings, emphasizing the complexity of exploring the psychological impact of online social behaviors. Literature [19] examined the association between adolescents' online social behaviors and their psychological indicators such as social acceptance, anxiety and depression through potential profile analysis, identified three psychological states: prosperous, moderate and debilitated, and analyzed the differences in online behaviors among groups with different states, as well as examining the mechanisms of influence of online socialization on adolescent psychological well-being. Literature [20] approached the issue of adolescent mental health and its connections to online socialization with a longitudinal approach utilizing comparative analysis carried out in 2003 and 2015, it was pointed out that the depressive symptoms of adolescent females were on the rise, and the association between online socialization duration and mental health was revealed in 2015, which emphasized the need to pay attention to the potential impact of online socialization on adolescents' psychology. Literature [21] explored the relationship between early online social interactions of adolescents and their mental health, examined the distribution and gender differences of self-esteem and depressive symptoms in interactive networks through longitudinal online behavioral data, and pointed out that compared to older adolescents, their mental health is likely to be less affected by social influences,

emphasizing the complex role of environmental factors on early psychological development. The literature [22] has assessed the impact of socialization in the online world on mental health of adolescents by conducting an analysis of 23 independent research works, highlighting the fact that there exists a complex two-way relation between the above phenomena. The study focused on the role of protection that social relations in the online environment may play, pointing at significant differences in patterns of using social media among genders, and highlighting the advantages and disadvantages of digital communication that provide ample opportunities for social support but also have the potential for social comparison.

Moreover, Literature [23] analyzed the link between adolescent social behavior online and mental health outcomes by synthesizing the findings from several studies, noting that most of the existing studies are correlational and often have conflicting conclusions, and emphasizing that the most recent large-scale studies have shown an association that exists but with a small impact and lack of evidence of causality. Literature [24] provided an insight into the complicated connection between online socialization and mental health of teenagers, emphasizing the existence of both positive and negative associations between the phenomena, and the importance of contextual understanding. Literature [25] examined systematically the influence of social technologies on adolescent mental health, reporting a number of benefits associated with the online environment, such as improved self-esteem and increased social support options, as well as risks such as cyberbullying and depression, and emphasizing that most of the studies have mixed conclusions, and there is still a lack of conclusive evidence of causation, so that the design of relevant studies needs to be strengthened in the future. Literature [26] examined the joint impact of online social addiction and online gaming disorders on mental health in adolescents, and by analyzing the interactions between the two, pointed out that they may uniquely exacerbate mental distress, and emphasized the need to consider the potential role of sociodemographic and technological variables. Researches [27] have confirmed that overuse of smartphone and social media platforms among teens aggravates psychological problems and increases tendencies towards self-harm causing serious negative impacts on the psychological well-being, academic success and social adaptation of adolescents via the processes of social comparison, cyberbullying and sleep disturbances among others with teen girls being more affected than boys. Research [28] focuses on how school nurses may help in handling the psychological crises caused by the online social interactions of adolescents, and states that in addition to minimizing the negative impact of social media on the mental health of teenagers, nurses should also teach teachers and pupils about the symptoms of mental disorders and self-injuries and provide proper advice.

This paper is dedicated to identifying the psychological states of adolescents' online social behaviors through physiological signals and designing an early warning system for adolescents' early psychological crises. In this paper, the physiological mechanisms of psychological state changes are firstly explored, and based on this, a requirement analysis is conducted for the multimodal data acquisition system, and the overall scheme of the system is designed according to the proposed requirements. According to the characteristics of physiological signals and external interference, the wavelet transform is used to pre-process them, and the sampled signals obtained are further feature extracted. Finally, a psychological state recognition model based on improved PSO-BP neural network is proposed to recognize the psychological state of the experimental subjects, and a mental health early warning system is proposed to make a judgment on the psychological condition of the adolescents and issue a psychological warning in time.

2 Basic Theory of Physiological Signaling

2.1 Electrocardiographic signals

ECG signal is a kind of signal with nonlinearity, non-stationarity and randomness, its amplitude is very weak, and it is easy to be overwhelmed by all kinds of external noise. It has a wide frequency range, in which the signal energy is mainly concentrated at 0.5Hz-50Hz.

The standard ECG during one cardiac cycle consists of the following waves and segments: P, Q, R, S, T waves and RR, PR, QRS and ST intervals respectively. The locations of the above waves and segments in the ECG signal and their importance are described in Table 1 below.

Table 1: Position and meaning of the electrical signal

Band	Position	Meaning
P	First wave of electrocardiogram	Left atrium and the right atrium are polarized
PR	Period before the QRS wave group after the P wave	Time of the atrium to polarization to the ventricle
QRS	Steep waveform after the p wave	Left ventricle and the right ventricle are polarized
RR	Between two R waves	One cardiac cycle
ST	QRS wave group goes back to the R wave	Ventricular depolarization is slow and slow
T	Long waveform of the QRS wave group after duration	Ventricular rapid multipole

2.2 Electroencephalographic signals

EEG signal is also a signal with non-linearity, non-stationarity and randomness. Compared with ECG signals, the amplitude of EEG signals is much weaker, usually below 10 μV, with a maximum amplitude of 100 μV, and the frequency of the signals is lower, distributed between 1 Hz and 50 Hz. The waveforms of EEG signals are irregular, and according to their frequency, amplitude and physiological characteristics, they can be classified as $delta(\delta)$, $theta(\theta)$, $alpha(\alpha)$, $beta(\beta)$ and $gamma(\gamma)$ five rhythmic waves, as shown in Figure 1.

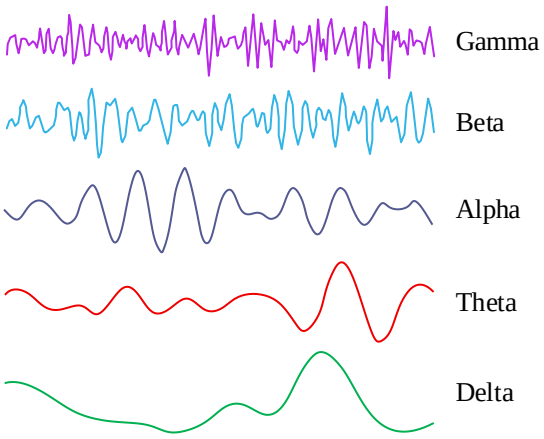

Figure 1: Brain electrical signal rhythm wave

The characteristics of each rhythmic wave of the EEG signal are shown in Table 2.

Table 2: Brain electrical signals each rhythm

Rhythm wave	Amplitude(μV)	Frequency(Hz)	Behavior
δ wave	20~200	1~4	Sleeping, Sleeping
θ wave	100~150	4~7	Quiet, Meditation
α wave	20~150	8~12	Relax
β wave	5~150	12~25	Focus, Alert
γ wave	<5	>25	Excitement

2.3 Oxygen saturation

Blood oxygen saturation (SpO2) is defined as the proportion of oxygenated hemoglobin (HbO2) relative to the total volume of all hemoglobin capable of binding oxygen (Hb), and is expressed through the following formula:

$$SpO_2 = \frac{c_{HbO_2}}{c_{HbO_2} + c_{Hb}} \tag{1}$$

Oxygen saturation serves as a physiological parameter that characterizes the capacity of the blood to transport and deliver oxygen to bodily tissues. Oxygen saturation is around 95% in normal adults and can be slightly below the normal range at high altitudes or in certain disease states. In a healthcare setting, oxygen saturation can be used to monitor a patient's respiratory status, assess respiratory and circulatory function, and cardiovascular health, among other things.

Measurement of oximetry is usually based on the photovoltaic volumetric pulse wave method, which is based on Lambert's law, which is based on the principle that oxygenated and reduced hemoglobin in the blood have different absorption properties for different wavelengths of light, and thus obtains the value of oximetry.

The absorption of light by the non-arterial component is constant, resulting in a direct current component (DC), whereas the absorption of light by the blood varies with the pulsation of the arterial vasculature, resulting in an alternating current component (AC). Absorption of light is greatest when vasodilation is greatest and blood volume is highest, when the intensity of outgoing light is lowest. Conversely, when vasodilation is minimal, the amount of light absorbed is lowest and the intensity of the ejected light is highest.

Based on Lambert's law, when monochromatic light at a wavelength of λ and an initial intensity of I_0 is directed onto human tissue, and arterial wall movement is assumed to be absent, the resulting reflected light intensity consists solely of the DC component I_{DC}. Its value is governed by the expression below:

$$I_{DC} = I_0 \cdot F \cdot e^{-\left(\varepsilon_{HbO_2} c_{HbO_2} + \varepsilon_{Hb} c_{Hb}\right) \cdot L} \tag{2}$$

In this expression, I_0 denotes the incident light intensity and F refers to the absorption coefficient characteristic of human tissue. The terms ε_{HbO_2} and ε_{Hb} are the absorption coefficients of oxygenated hemoglobin HbO2 and deoxygenated hemoglobin Hb, respectively, within the illuminated region of the tissue. Correspondingly, c_{HbO_2} and c_{Hb} represent the concentrations of oxygenated hemoglobin HbO2 and deoxygenated hemoglobin Hb present in the tissue. The variable L denotes the length of the optical path.

Cardiac contraction drives rhythmic expansion and contraction of the blood vessels. This vascular pulsation produces a variation ΔL in the optical path length, causing the reflected light intensity to comprise both a DC component and a superimposed AC component, expressed together as $I_{DC}+I_{AC}$. The relationship is described by the formula that follows:

$$I_{DC}+I_{AC}=I_0\cdot F\cdot e^{-\left(\varepsilon_{HbO_2}c_{HbO_2}+\varepsilon_{Hb}c_{Hb}\right)(L+\Delta L)} \tag{3}$$

Substituting Eq. (2) into Eq. (3) has:

$$I_{DC}+I_{AC}=I_{DC}\cdot e^{-\left(\varepsilon_{HbO_2}c_{HbO_2}+\varepsilon_{Hb}c_{Hb}\right)\Delta L} \tag{4}$$

Morphing the above equation to find the logarithm has:

$$\ln\left(\frac{I_{DC}+I_{AC}}{I_{DC}}\right)=-\left(\varepsilon_{HbO_2}c_{HbO_2}+\varepsilon_{Hb}c_{Hb}\right)\Delta L \tag{5}$$

Since I_{AC} is much smaller than I_{DC}, I_{AC}/I_{DC} can be regarded as infinitesimally small, so there:

$$\ln\left(\frac{I_{DC}+I_{AC}}{I_{DC}}\right)\approx\frac{I_{AC}}{I_{DC}} \tag{6}$$

Substituting equation (6) into equation (5) has:

$$\frac{I_{AC}}{I_{DC}}=-\left(\varepsilon_{HbO_2}c_{HbO_2}+\varepsilon_{Hb}c_{Hb}\right)\Delta L \tag{7}$$

Since the variable ΔL is unknown, it needs to be eliminated. Using two beams of light of different wavelengths to irradiate separately, set the wavelengths of these two beams of incident light as λ_1 and λ_2, respectively, which can be obtained from Eq. (7):

$$\frac{I_{AC}^{\lambda_1}}{I_{DC}^{\lambda_1}}=-\left(\varepsilon_{HbO_2}^{\lambda_1}c_{HbO_2}+\varepsilon_{Hb}^{\lambda_1}c_{Hb}\right)\Delta L \tag{8}$$

$$\frac{I_{AC}^{\lambda_2}}{I_{DC}^{\lambda_2}}=-\left(\varepsilon_{HbO_2}^{\lambda_2}c_{HbO_2}+\varepsilon_{Hb}^{\lambda_2}c_{Hb}\right)\Delta L \tag{9}$$

Dividing equation (8) by equation (9) has:

$$R=\frac{\varepsilon_{HbO_2}^{\lambda_1}c_{HbO_2}+\varepsilon_{Hb}^{\lambda_1}c_{Hb}}{\varepsilon_{HbO_2}^{\lambda_2}c_{HbO_2}+\varepsilon_{Hb}^{\lambda_2}c_{Hb}} \tag{10}$$

Substituting Eq. (10) into Eq. (2) simplifies to obtain:

$$SpO_2 = \frac{\varepsilon_{Hb}^{\lambda_2}}{\varepsilon_{HbO_2}^{\lambda_1} - \varepsilon_{Hb}^{\lambda_1}} \cdot R - \frac{\varepsilon_{Hb}^{\lambda_1}}{\varepsilon_{HbO_2}^{\lambda_1} - \varepsilon_{Hb}^{\lambda_1}} \tag{11}$$

In the above equation, $\varepsilon_{HbO_2}^{\lambda_1}, \varepsilon_{Hb}^{\lambda_1}, \varepsilon_{HbO_2}^{\lambda_2}, \varepsilon_{Hb}^{\lambda_2}$ are all constants, and it is sufficient to measure the DC and AC portions of the reflected light intensity for the two wavelengths of light separately, i.e., $I_{AC}^{\lambda_1}, I_{DC}^{\lambda_1}, I_{AC}^{\lambda_2}, I_{DC}^{\lambda_2}$, the bleeding oxygen saturation can be calculated.

In practice, due to the differences between human tissues, the empirical oxygen saturation calculation formula is obtained according to the method of experimental statistics:

$$SpO_2 = AR^2 + BR^2 + C \tag{12}$$

2.4 Electrical skin signals

Galvanic Skin Response (GSR) is the term used to describe the amount of electricity conducted by the skin, and the galvanic skin signal is otherwise called galvanic skin activity. The galvanic skin response is a direct indicator of the activity of the intrinsic sympathetic nervous system, as well as reflecting the level of alertness and cerebral arousal.

Since the electrodermal signal is an indirect measure of the sympathetic nervous system and is regulated by multiple regions of the brain, changes in the electrodermal signal can be induced by external stimuli or different psychological states, such as emotional arousal, fatigue, increased cognitive load, loud noises, bright light, etc. It is the only physiological indicator that is not influenced by the parasympathetic nervous system, and is therefore widely used in the study of different psychological states, such as stress, emotion, fatigue, and cognitive load.

2.5 Body temperature signals

Body temperature signals are temperature changes on the surface or inside the body. It is generally monitored through wearable devices and sensors. Variations in body temperature are important indicators of the physiological state of the body. In case the body experiences any emotional arousal or disturbance, there will be a variation in body temperature due to the activity of the sympathetic nervous system. Meanwhile, the collection of body temperature signal is relatively simple compared with other physiological signals, which can be realized only through wearable devices or sensors. Moreover, the body temperature signal can be combined with other physiological signals to form a psychological crisis early identification system, which further improves the accuracy and reliability of psychological identification.

The body temperature signal is one of the physiological parameters which can be obtained based on the thermal variations experienced either on the surface of the body or inside the body of humans. Changes in body temperature signals are closely related to emotions, and emotional fluctuations affect blood circulation in the human body, which in turn leads to changes in body temperature. A great deal of physiologically significant information can be gathered through body temperature signals. Using the method of feature extraction, the elements that are important for recognizing emotions can be selected from the body temperature data. Feature extraction has been performed using different techniques on body temperature signals; however, the most common among these techniques fall under three broad categories: time domain, frequency domain, and time-frequency domain.

3 Multimodal data acquisition system design

3.1 Needs analysis

The multimodal data acquisition equipment designed in this paper is positioned to collect data during the psychological assessment of the adolescent population, and the important physiological signals such as ECG, EEG, oximetry, picoelectricity, temperature data can be recorded in real time while audio and video recordings are simultaneously being done. As far as the entire system goes, the following requirements are proposed.

(1) The device needs to realize the acquisition of five physiological signals, namely, ECG, EEG, oximetry, picoelectricity and body temperature, as well as the acquisition of two non-physiological signals, namely, video and voice. The size of the device should be small enough to capture more realistic data without attracting the attention of the subject in some scenarios.

(2) The host computer software needs to plot ECG, EEG and DT signals into graphs for real-time display, display oxygen saturation and body temperature in real-time in numerical form, the live picture provided by the camera is displayed in real time on the display and all recorded data are saved for further processing.

(3) For the collected ECG signals, clear QRS wave clusters should be observed, and the baseline is smooth. For the acquired EEG signals, clear δ, θ, α, β and γ waves should be observed. For the acquired electrodermal signals, the trend of the electrodermal response should be clearly observed. For the collected oxygen saturation and heart rate, the accuracy should meet the requirement of ±2.5% accuracy compared with professional equipment.

3.2 Overall program design

Based on the requirements stated above, the design of a system that would help acquire the above-mentioned data has been proposed. The architecture of the developed system is shown in Fig. 2. The hardware portion of the system comprises seven different blocks, each corresponding to one of the following stages of data acquisition: power supply module, ECG acquisition module, EEG acquisition module, blood oxygen and pulse acquisition module, picoelectricity acquisition module, body temperature module, video and voice acquisition module. Among them, the video and voice modules can directly use USB to communicate with the host computer, the temperature module, ECG module and EEG module support serial communication, so they can directly communicate with the host computer through RS232, while the blood oxygen, pulse module and skin electric module need to use a microprocessor, and then communicate with the host computer through RS232. Eventually, the host computer will display all the collected data in the form of texts and graphs on the software interface, allowing users to observe the state of the system in real-time mode. The software also has the feature of controlling and configuring data acquisition devices via the software interface.

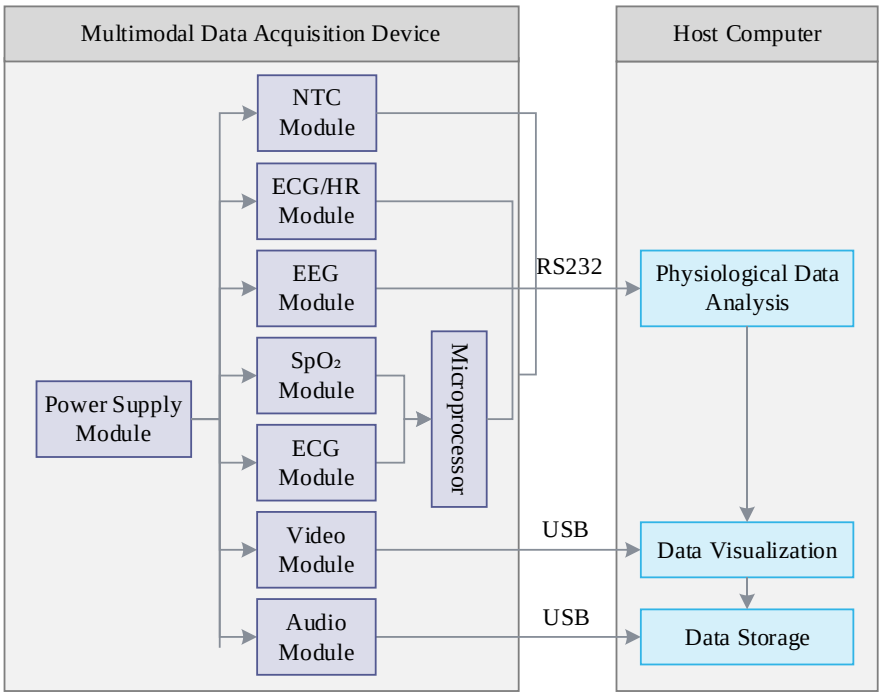

Figure 2: Multi-modal data acquisition system overall structure

4 Physiological signal processing

There are many processing methods for physiological signals, such as Fourier transform, wavelet transform and so on. In this paper, the wavelet transform method is used in the subsequent physiological signal processing for feature acquisition and analysis, and the related wavelet transform processing method is explained below.

4.1 Continuous wavelet transform

The Fourier transformation approach is extensively used in signal analysis since it can be considered an important tool to create a relevant relationship between two ways of representing a signal, namely the time-domain way and the frequency-domain way. From the point of view of theory, the approach allows for projecting a signal onto a frequency-domain function. This is possible due to the fact that the approach switches the analysis of the signal from one domain to another. Therefore, the analysis can provide some frequency features of the signal under consideration. The applicability of the approach is remarkable as well, because it can analyze both periodic and non-periodic signals, which have a finite amount of energy. Consequently, it can be utilized effectively in various fields, including signal and image processing. However, the spectrum obtained by means of the transformation cannot represent local properties of a signal.

The wavelet analysis technique is applied by considering the time-frequency localization approach which uses windows of fixed size but varying shape. The wavelet technique provides high frequency resolution when low frequencies are considered and poor temporal resolution; whereas high temporal resolution and poor frequency resolution are provided in the case of high frequencies. This way, the signal can be improved and its features are determined by using the wavelet approach. Compared to other traditional signal analysis techniques, the wavelet method provides a slight edge in motion artifact suppression and baseline drift reduction.

Suppose the wavelet function is $\psi(t)$, subject to the following admissibility condition:

$$C^{\psi} = \int_R \frac{|\psi^*(\omega)|}{|\omega|} d\omega < +\infty \tag{13}$$

Designating $\psi(t)$ as the mother wavelet or wavelet basis, a family of functions is generated through successive translation and dilation operations:

$$\psi_{a,\tau}(t) = \frac{1}{\sqrt{a}} \psi\left(\frac{t-\tau}{a}\right) \quad a, \tau \in R, a \neq 0 \tag{14}$$

The resulting functions $\psi_{a,\tau}(t)$ form a complete set of orthogonal bases spanning the square-integrable space $L^2(R)$. For any function $f(t) \in L^2(R)$, the wavelet transform is expressed as:

$$Wf(a,\tau) = \langle f, \psi_{a,\tau} \rangle = \int_{-\infty}^{+\infty} \psi_{a,\tau}(t) f(t) dt \tag{15}$$

Here, a is referred to as the scale factor. Wavelet transforms computed at small scales capture the high-frequency components of the signal, whereas transforms at large scales correspond to contains the low-frequency components of the signal. τ is the translation factor, which is a coefficient about time and determines the time domain information of the wavelet transform, because the change of the two values presents a continuous state, so $\psi_{a,\tau}(t)$ is called the continuous wavelet basis function.

When $f(t)$ meets the square-integrability requirement such that $f(t) \in L^2(R)$, the corresponding continuous wavelet transform can be written in the form below:

$$WT_f(\alpha,\tau) = \langle f(t), \psi_{a,\tau}(t) \rangle = \frac{1}{\sqrt{\alpha}} \int_R f(t) \psi^*\left(\frac{t-\tau}{\alpha}\right) dt \tag{16}$$

In this expression, $\psi(t)$ represents the chosen wavelet function and $\psi^*(t)$ is its complex conjugate counterpart. Both $\alpha = 0,1,\tau$ and τ are treated as parameters taking continuous values.

Reformulating the above as a convolution yields:

$$WT_f(\alpha,\tau) = \frac{1}{\sqrt{\alpha}} \int_R f(t) \psi^*\left(\frac{t-\tau}{\alpha}\right) dt = |\alpha|^{1/2} f * \bar{\psi}_{|\alpha|}(\tau) \tag{17}$$

where $\bar{\psi}_{|\alpha|}(\tau) = |\alpha|^{-1} f * \psi^*_{|\alpha|}(-\tau/\alpha)$. From an engineering standpoint, the operator $\bar{\psi}_{|\alpha|}(\tau)$ functions as a high-pass filter applied to the input signal.

4.2 Discrete Wavelet Transform

Within the continuous wavelet transform, the scale factor a and the translation factor τ each assume values over a continuous range, placing a heavy demand on computational resources. Beyond this concern, data handled by numerical platforms such as MATLAB exists inherently in discrete form, which makes discretization of both a and τ a practical necessity. The steps involved in this discretization are outlined below:

Let $\alpha = \alpha_0^j$, $\tau = k\alpha_0^j b_0$, and assume $\alpha_0 > 1$.

Then the wavelet sequence formula is:

$$\psi_{j,k}(t) = \frac{1}{\sqrt{\alpha_0^j}} \psi\left(\frac{t - k\alpha_0^j b_0}{\alpha_0^j}\right) = \alpha_0^{-\frac{j}{2}} \psi\left(\alpha_0^{-j} t - k b_0\right),\ j,k \in Z \tag{18}$$

And the discrete wavelet transform coefficients can be expressed as:

$$C_{j,k}(f, \psi_{j,k}) = \sum_{n=-\infty}^{\infty} f(t) \psi_{j,k}^*(t) \tag{19}$$

where $\psi(t)$ represents a wavelet basis function that must conform to a well-defined set of mathematical conditions.

The formula through which the original signal is reconstructed from its discrete wavelet coefficients is stated as:

$$f(t) = \sum_{j=-\infty}^{\infty} \sum_{k=-\infty}^{\infty} C_{j,k} \psi_{j,k}(t) = \sum_{j=-\infty}^{\infty} f_j(t) \tag{20}$$

The family of basis elements $\psi_{j,k}(t) = 2^{-j/2} \psi\left(2^{-j} t - k\right)$ spans the space of discrete wavelet functions. Both j,k are restricted to integer values: j controls the discretized scale level through the relation $\left(\alpha = \alpha_0^j\right)$, while k governs the discrete temporal displacement via $\left(\tau = k\tau_0\right)$. The variable t remains defined over a continuous domain. Within this framework, $f(t)$ isolates the portion of the signal f(t) residing at resolution level j.

4.3 Wavelet Denoising

The physiological signals obtained from laboratory acquisition are not ideal signals, and there are many noises and interferences, mainly as follows:

(1) Industrial frequency interference. The range of industrial frequency interference is generally around 50~60Hz, which is mainly caused by the contact between the AC power supply, sensors, electrode pads and other devices and the human body, causing burrs in the signal waveform.

(2) Baseline drift. Baseline drift is a low-frequency interference, usually less than 1Hz, generally due to the signal acquisition process of human behavioral actions or breathing, electromyography, skin temperature and many other factors. Baseline drift on the physiological signal waveform interference, will cause the waveform up and down.

(3) EMG interference. Myoelectric interference is caused by the muscle tension of the test subject, with a wide range of frequencies, which makes the signal show frequent irregular disturbances and affects the experimental results.

(4) Electromagnetic interference. Electromagnetic interference is usually caused by the cell phone, watch or other peripherals carried by the test subject.

(5) Electrode contact noise. When there is a poor contact condition between the human body and the electrodes, a certain electrode contact noise will be generated, which usually causes the signal baseline to jump.

(6) Motion artifacts. The acquisition of physiological signals may also result in the addition of noise due to any small motion made by the individual under investigation. This type of noise

falls within a frequency band less than 7 Hz and can cause slight changes in the signal baseline level.

(7) Random noise. Random noise in the environment and internal noise of the instrument, etc. will also have an impact on the acquired signal.

The underlying principle of wavelet denoising is mainly based on the two inherent characteristics of wavelets: their low entropy feature and their multiresolution characteristic. Based on these two features, physiological signals are then decomposed at several scales. By using the different frequency distributions of physiological signals and noises, the two can be separated and processed individually. In general, physiological signals generated from the body are usually low-frequency signals with relatively constant waveform structures, while noises are high-frequency signals with sudden changes. According to the different nature of the two, the original signal can be effectively decomposed into two parts: high-frequency and low-frequency. At present, the wavelet denoising method is mainly divided into three kinds of methods, respectively, the threshold method, the mode great value method and the translation invariant method. Each of the three methods has its own advantages and disadvantages, and has been widely used in different fields. Among them, the thresholding method has the advantage of retaining the features at the signal mutation points, so it is often chosen to deal with all kinds of physiological signals. The main principle of denoising using the threshold method is that when the original signal is effectively decomposed by the wavelet transform, the noise signal is separated from the target signal. Since the energy of the target signal is much larger than that of the noise signal, its corresponding wavelet coefficient is correspondingly larger. On this basis, an appropriate threshold can be established for the discrepancy between wavelet coefficients, serving the purpose of separating noise components from the signal of interest. Once this step is complete, wavelet reconstruction is performed to recover the cleaned target signal.

The magnitude of the threshold is determined by taking the absolute value of the high-frequency wavelet coefficients at each corresponding decomposition level. Two distinct thresholding strategies exist: the soft threshold and the hard threshold. Let w denote the original high-frequency wavelet coefficients, λ represent the chosen threshold value, and w_λ denote the revised high-frequency coefficients produced after wavelet decomposition and subsequent threshold quantization. In the case where $|w| \geq \lambda$, soft threshold denoising assigns the new wavelet coefficient as the signed difference between the original coefficient and the threshold, whereas hard threshold denoising retains the original high-frequency wavelet coefficients without modification. In the case where $|w| < \lambda$, both strategies set the high-frequency wavelet coefficients to zero.

The quantization rule governing soft threshold processing is stated as:

$$w_\lambda = \begin{cases} [sign(w)](|w| - \lambda) & |w| \geq \lambda \\ 0 & |w| < \lambda \end{cases} \tag{21}$$

The quantization rule governing hard threshold processing is stated as:

$$w_\lambda = \begin{cases} w & |w| \geq \lambda \\ 0 & |w| < \lambda \end{cases} \tag{22}$$

5 Early Psychological Crisis Recognition Model

5.1 Improved particle swarm optimization algorithm

(1) Principle of Particle Swarm Algorithm

PSO algorithm is a kind of behavioral research originated from birds' foraging, used to solve optimization problems, its basic principle is: when in each problem that needs to be optimized, one of its solutions is a particle in the search space, and each particle corresponds to a value of fitness, and the function model of fitness is also the function model that is being optimized, in addition, the speed produced by the particle during the search process can determine its direction and distance, when the direction and distance are determined, the particle can keep searching through the direction and distance until the optimal value is found.

Suppose the number of input features is D, and the population contains m individuals in total. The velocity of the i th particle is expressed as $V_i = \left(v_{i1}, v_{i2}, v_{i3}, \cdots, v_{iD}\right)^T$, and its position in the search space is given by $X_i = \left(x_{i1}, x_{i2}, x_{i3}, \cdots, x_{iD}\right)^T$. At any given point in the search process, the position of a particle constitutes a candidate solution to the problem under consideration. The procedure involves first constructing the fitness function, then computing the fitness value for each particle, and subsequently identifying the optimal solution through pairwise comparison of all individual fitness values.

The best position encountered by the i th particle throughout its search history is denoted as $Pbest_i = \left(pbest_{i1}, pbest_{i2}, pbest_{i3}, \cdots, pbest_{iD}\right)^T$. The global best position attained by the entire population is determined by comparing the personal best positions of all particles, yielding $Gbest = \left(gbest_1, gbest_2, gbest_3, \cdots, gbest_D\right)^T$. Once the optimal values of both $Pbest$ and $Gbest$ have been identified, the next generation of particles is produced by applying Equations (23) and (24). This computational cycle is then repeated iteratively until a satisfactory optimal solution is reached.

$$\begin{aligned} V_i^{n+1} = V_i^n + C_1 \times rand_1() \times \left(Pbest_i - X_i^n\right) \\ + C_2 \times rand_2() \times \left(Gbest - X_i^n\right) \end{aligned} \tag{23}$$

$$X_i^{n+1} = X_i^n + V_i^n \tag{24}$$

Here, C_1 and C_2 serve as learning factors, while $rand_1()$ and $rand_2()$ are randomly generated vectors whose values fall within the interval [0, 1]. The term V_i^n refers to the velocity of the i th particle at the n th iteration, and X_i^n denotes the position of the i th particle at the n th iteration.

(2) Improved particle swarm optimization algorithm

The basic particle swarm optimization algorithm carries several inherent weaknesses that become apparent during practical application. It has a pronounced tendency to converge prematurely, stagnate at local optima, and exhibit early maturity in its search behavior, all of which compromise solution quality and introduce substantial error into the final output. To address these deficiencies, this paper proposes a series of targeted modifications to the foundational algorithm. In the PSO framework, the path each particle traces through the solution space is jointly determined by two learning factors, C_1 and C_2. The factor C_1 weights

the influence of a particle's own historical experience, while C_2 reflects the guidance exerted by the broader population. Together, these two parameters regulate the flow of information across the swarm, embodying the cooperative learning mechanism that lies at the heart of the PSO approach. Therefore, when the learning factor C_1 is set large, the particles will keep wandering in a range and it is difficult to continue the search. When the learning factor C_2 is set large, it will cause the particles to converge to the local minimum prematurely. To address this problem, this paper introduces a PSO model with a contraction factor, which utilizes the contraction factor φ, which not only removes the boundary restriction on the speed, but also selects the appropriate parameters to ensure the convergence of the PSO algorithm, and the improved PSO algorithm searches for the optimal value faster and more accurately than the basic PSO algorithm.

The updated velocity equation and the corresponding contraction factor expression are given in (25) and (26) respectively.

$$V_i^{n+1} = \varphi\left[V_i^n + C_1 \times rand_1() \times \left(Pbest_i - X_i^n\right) + C_2 \times rand_2() \times \left(Gbest - X_i^n\right)\right] \tag{25}$$

$$\varphi = \frac{2}{\left|2 - C - \sqrt{C^2 - 4C}\right|}, C = C_1 + C_2, C > 4 \tag{26}$$

In these expressions, φ denotes the contraction factor, which regulates the flight speed of particles operating under positional constraints. The term C represents the combined learning factor. Through a comparative evaluation of different parameter configurations, the population size in this study is set to 100, and both learning factors are assigned equal values such that $C_1 = C_2 = 2.5$. On this basis, the improved PSO algorithm is adopted to train and optimize the classifier developed in this paper. The flowchart describing the operational procedure of the improved PSO algorithm is provided in Fig. 3.

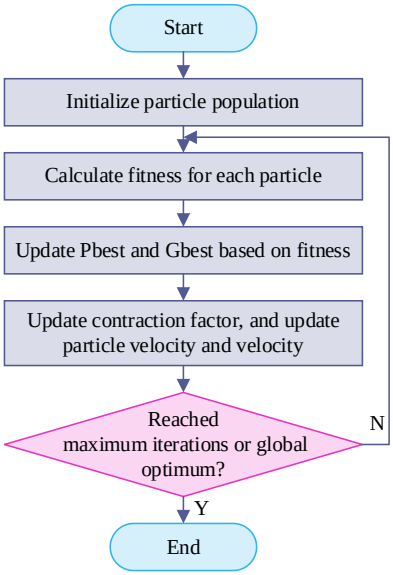

Figure 3: Improves the flow chart of the PSO algorithm

5.2 Introduction to Artificial Neural Networks and BP Network Models

In the last two years with the increasing prevalence of artificial intelligence, neural networks have become the most widely used algorithm in machine learning. The network model of Artificial Neural Network (ANN) is a model that simulates the human brain in processing information. It is modeled as a multiple-input, single-output model with many nodes, i.e., neurons, connected to each other, and each input signal has a weight value. In order to make the output signal unaffected by certain factors, then a bias will be added to it, at which point the input signal after summation will be output through the transfer function $f()$. The mathematical model can be expressed by equations (27), (28).

$$net_j = \sum_{i=1}^{n} w_{ij} x_i - \theta \tag{27}$$

$$y_j = f\left(net_j\right) \tag{28}$$

If the bias is viewed as a weight w_{0j} with input $x_0 = -1$, the above equation can be simplified as:

$$net_j = \sum_{i=1}^{n} w_{ij} x_i \tag{29}$$

Artificial neural network is like the human brain with certain learning ability, its learning process is to input the known number of training samples into the network, the continuous process of updating the values of weights and thresholds in the network takes place as a result of repeated calculations in response to the input, which eventually leads to generation of the required output signal. The neural networks differ from each other in their ability to perform nonlinear operations and their distributed parallel computation model, but also has the advantages of strong self-learning ability as well as robustness, so according to the learning rules of neural network, it can be used for intelligent recognition more effectively. At present, there are many neural network models, and the most widely used is the BP neural network with simple structure, strong stability and certain operability, which is why the BP neural network algorithm is applied to classify data in the current study.

BP neural network is a multi-layered feed-forward neural network structure, where information flow takes place in only one direction. The learning process of the BP neural network can be described as follows. First, connections among input neurons are established by assigning weights. The input signals are summed up, and the sum is then applied to the activation function and undergoes thresholding for the output value to be sent to the hidden layer as input. Similarly, signals in the hidden layer are processed and sent to the output layer, where the output is obtained from the network. For backpropagation, the output from the output layer is measured against the expected output using an error function. In case the error does not meet the required tolerance level, the process is carried out in reverse, and the weights and thresholds are updated in the negative gradient direction. The above process is repeated continuously until the difference between the actual output from the BP network and the expected output is within an acceptable range.

5.3 Mental State Recognition Model Based on Improved PSO-BP

The advantage of BP neural network is that it can learn and store a large number of input to

output pattern mapping relationships without knowing the mathematical equations of the input to output mapping relationships. However, for BP neural networks, the weights and thresholds will greatly affect the training results during the training process of the network. On this basis, the present study employs the improved PSO algorithm as the mechanism for determining the optimal weights and thresholds of the BP neural network.

Applying the improved PSO algorithm to the optimization of a BP neural network requires the prior construction of a suitable fitness function model. The method by which fitness values are computed is presented in Equation (30). A smaller value of the fitness measure $Fitness_i$ indicates that the parameter optimization has achieved a more favorable outcome. Throughout the optimization search conducted via the improved PSO, the weights and thresholds of the BP network are encoded as the position vector X associated with each particle in the swarm.

$$Fitness_i = \frac{1}{K}\sum_{i=1}^{K}\sum_{j=1}^{M}\left(w_{j,i}^{d} - w_{j,i}\right)^2 \tag{30}$$

In this expression, K denotes the total number of samples and M represents the number of nodes contained in the output layer. The term $W_{j,i}^{d}$ refers to the ideal state value of the j th output layer node corresponding to the i-th sample, while $W_{j,i}$ designates the actual state value produced by the j th output layer network node for the i-th sample.

Once the fitness function has been successfully established, the advanced PSO-BP neural network method will be utilized in order to conduct psychological crisis prediction of the adolescent group. The detailed procedures for conducting psychological crisis identification with the help of the advanced PSO-BP neural network are given below:

Step 1: Read in the data of the features from the constructed dataset.

Step 2: Determine the numbers of neurons in each layer. 20 neurons should be set up in the input layer, 10 neurons should be allocated in the hidden layer, and 2 neurons should be specified in the output layer.

Step 3: Conduct data normalization of the input and output samples.

Step 4: Build up the network model and initialize all necessary parameters. The parameters needed to be initialized contain the numbers of particles in the advanced PSO algorithm as well as the initial positions and velocities of each particle.

Step 5: Identify the personal best position $Pbest$ recorded by each particle over the course of its search history, and designate the most favorable among all personal best positions as the global best value $Gbest$.

Step 6: Compute the adaptation value for every particle using Equation (30). For any particle whose current fitness surpasses its previously recorded individual best, update the corresponding $Pbest$ t value and recalculate the particle's position accordingly. Should any particle's individual best fitness value prove superior to the prevailing global best fitness value, update and recalculate the $Gbest$ value.

Step 7: Adjust the velocities and coordinate positions of all the particles in accordance with the corresponding formulas.

Step 8: Get the threshold and weight values of the BP network according to the iteration number judgment. If the number of iterations equals the predefined maximum, the iterations stop; otherwise, proceed to Step 5.

Step 9: Set the optimal initial threshold and weight values acquired from the advanced PSO algorithm to the BP network.

Step 10: Apply the optimized BP network to conduct early psychological crisis identification and obtain the recognition rate. Figure 4 illustrates the flowchart of the whole algorithm.

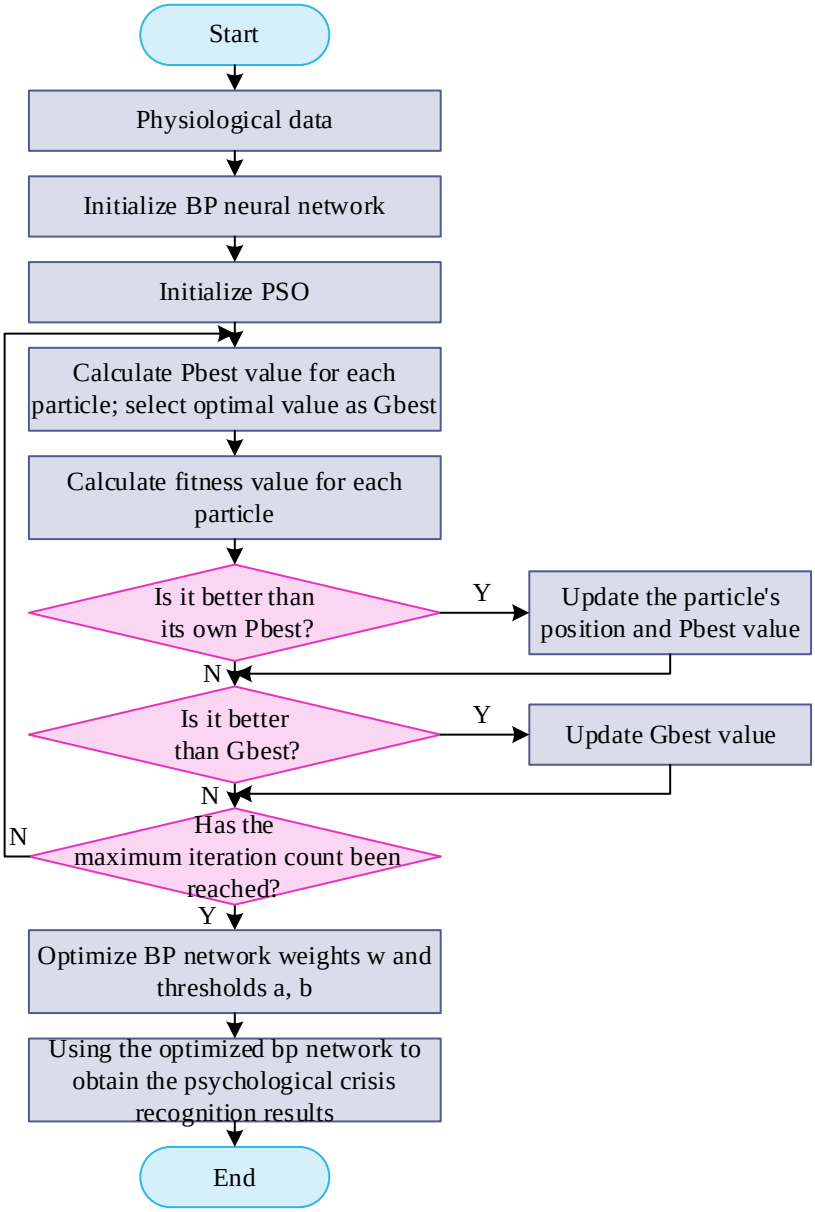

Figure 4: Flow chart for improved PSO-BP neural network

6 Physiological data preprocessing and reliability testing

The MP150 system designed by BIOPAC has become popular in many branches of sciences such as neuroscience, psychology, medicine, and artificial intelligence, because of the extensive functions and reliability that can be attributed to this device. In order to prove the validity of the physiological signals acquired by this system, the standard physiological signals input from the physiological signal source were firstly acquired by this system to test the quality of the signals acquired by the system, and then the physiological signals of the subjects when socializing on the Internet were acquired by this system and the MP150 system of BIOPAC

Company of the U.S.A. separately, and the characteristics of the waveform amplitudes, phases, and spectra were compared, so as to validate the physiological signals acquired by the system and the reliability of the system. Reliability. This chapter discusses the comparison test process of the system built in this experiment with that of the BIOPAC MP150 system.

6.1 EEG signal preprocessing and testing

The waveform of the resting state of EEG signal is depicted in Fig. 5. The waveform of the raw EEG signal obtained by the system used in this experiment is illustrated in Fig. 5(b), whereas the waveform of the EEG signal collected by the MP150 system in similar experiment environment is shown in Fig. 5(a). From Fig. 5(a) and Fig. 5(c), one can observe that the raw EEG signal is vulnerable to interference in the form of sharp peaks due to industrial noise at either 50Hz or 60Hz, physiological artifacts generated by the signals of ophthalmoelectricity, electromyography, and pulse, and small and slowly changing baseline drift caused by impedance changes of the electrodes on the surface of the skin in the process of acquisition.

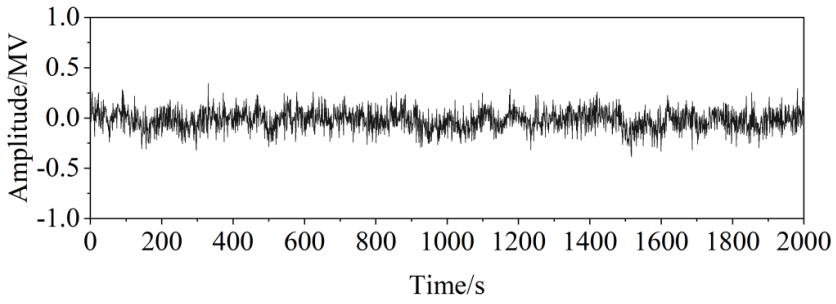

(a) Brain electrical signals collected by the mp150 system

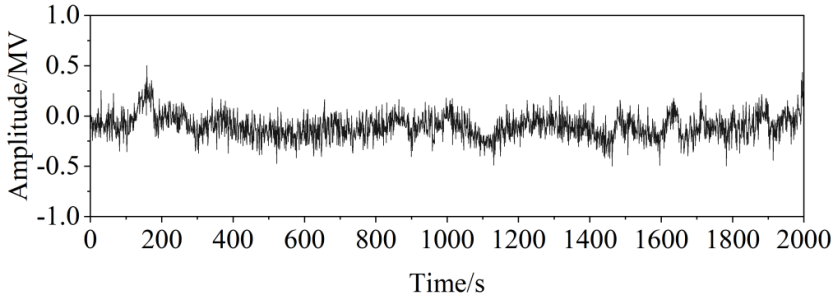

(b) State of the state of the state of the state of the brain

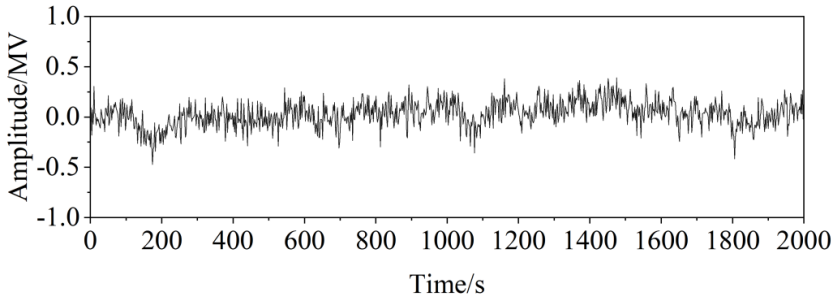

(c) Remove the brain electrical signals from the noise

Figure 5: Brain signal waveform contrast

In order to remove the interfering noise mixed in the original EEG signal, the signal is processed in this section using the preprocessing algorithm introduced in Chapter IV. In this paper, wavelet denoising algorithm is used to remove the physiological signals. Figure 5(c) shows the waveform of the signal after removing the noise. Comparison of the amplitude, phase and spectral characteristics of the signal in Fig. 5 can verify that this system acquires EEG signals accurately and efficiently.

6.2 Cardiac Data Preprocessing and Testing

The waveform of the resting ECG signal is shown in Fig. 6. The waveform of the ECG signal acquired using the system proposed in this research work is shown in Fig. 6(b), while the waveform of the ECG signal recorded using the MP150 system under identical experimental conditions is illustrated in Fig. 6(a). From Fig. 6(a) and Fig. 6(c), it is clear that in the course of acquiring ECG data, the signal gets corrupted by industrial frequency interference, electromyography, and baseline wandering, which occur concurrently.

In order to remove the effects of those interfering elements, the preprocessing method mentioned in chapter IV is used to pre-process the raw ECG signal. Since the frequency of EMG signal is higher than that of ECG signal and its waveform is characterized by irregular and rapid changes, it is very easy to be superimposed with the ECG signal and lead to bias in the calculation of heart rate, so this paper uses wavelet denoising algorithm to remove the noise. Baseline drift and 50Hz or 60Hz industrial frequency interference noise are similar to the removal method of this noise in the ECG signal. Figure 6(c) shows the signal waveform after removing the noise. Comparison of the amplitude, phase and spectral characteristics of the above waveforms can verify that the ECG signal acquired by this system is valid.

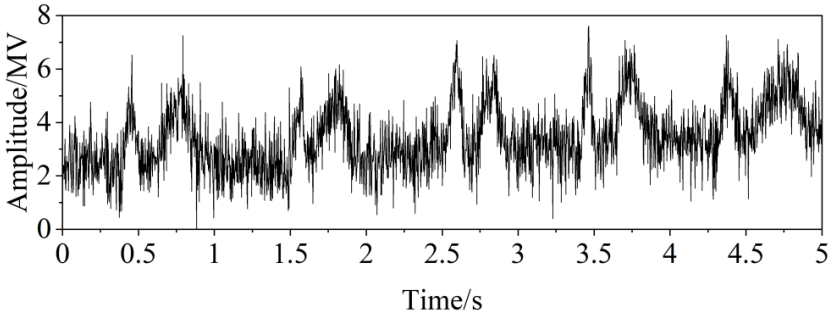

(a) MP150 collection of cardiac electrical signals

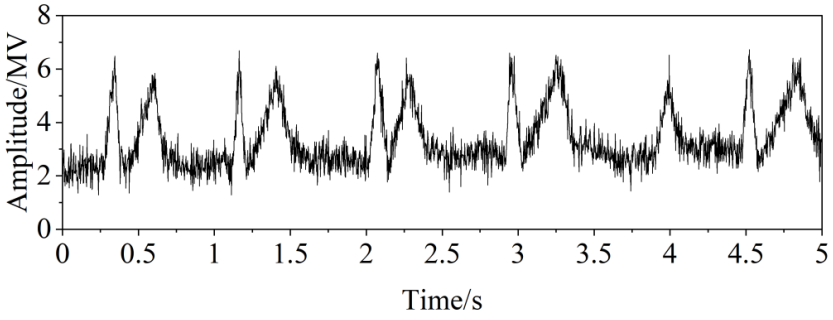

(b) Resting-state original electrocardiogram signal

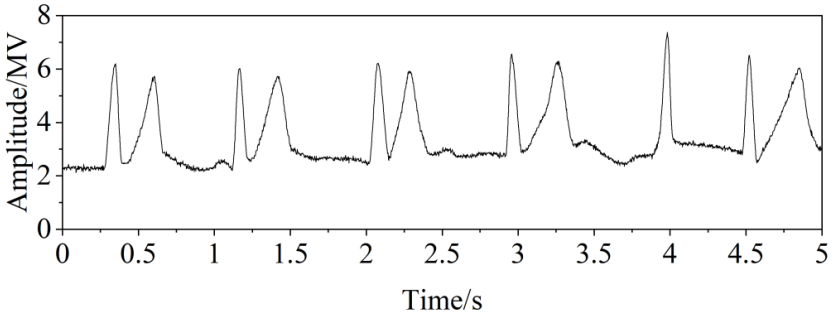

(c) Remove the signal from the noise

Figure 6: Contrast of signal waveform of cardiac electrical signal

Subsequently, the performance of heart rate calculations carried out by the proposed system is checked by generating ECG signals based on different heart rates through a physiological signal generator, and the simulated heart rates are compared with the heart rates obtained from ECG signal generated by this system through actual experiments. Results of the comparison analysis are tabulated in Table 3 below. It is evident from the table that there exists a deviation of 2% from the simulated value.

Table 3: Heart rate test data

Heart rate of analog signal source (beats/minute)	System measured the heart rate (beats/minute)	Error (%)
60	60	0.0
65	66	1.5
70	71	1.4
75	75	0.0
80	81	1.3
85	85	0.0
90	90	0.0
95	96	1.1
100	100	0.0
105	106	1.0
110	112	1.8
115	116	0.9
120	122	1.7

6.3 Picoelectric data preprocessing and testing

Figure 7 illustrates the waveform of the picoelectric signal. Figure 7(b) depicts the waveform of the picoelectric signal measured with the system designed in this research work, whereas Fig. 7(a) shows the waveform of the picoelectric signal measured using the MP150 system under similar experimental conditions. Since the amplitude of the EKG signal is larger than that of the EEG and ECG signals, the interfering noises that have a greater impact are mainly motion artifacts caused by the movement of the contact surface between the surface electrodes and the skin, and crosstalk to the source signal from the EKG signals of non-measured muscle groups.

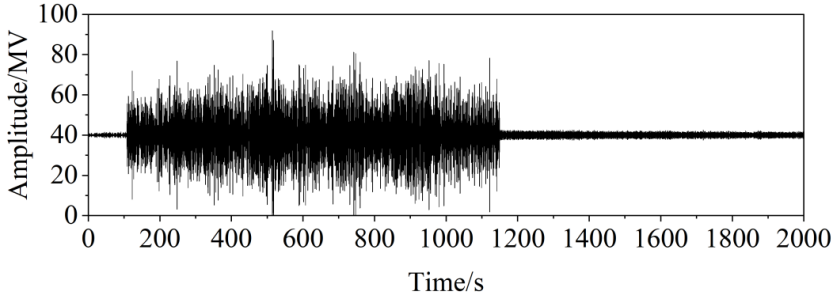

(a) MP150 obtained skin signal

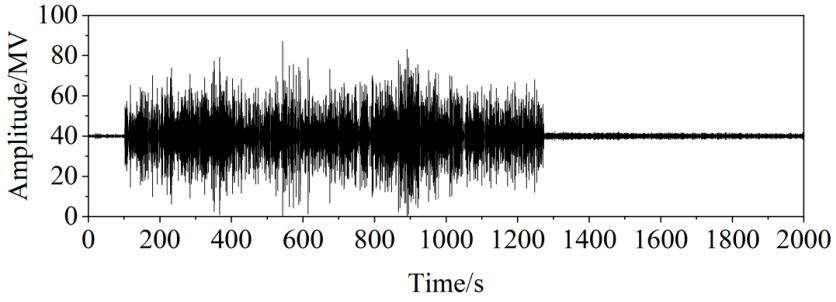

(b)Static state raw

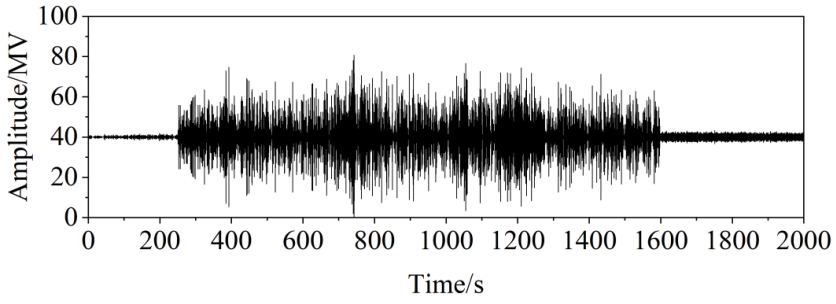

(c)Remove the acoustic signal after noise

Figure 7: Contrast of signal waveform

In order to filter out the unwanted noise from the picoelectric signal, the physiological data processing algorithm mentioned in Chapter IV is used in this segment of the discussion. Since the frequency of motion artifacts and crosstalk mixed in the PEEK signal is usually below 20 Hz, a weighted sliding window filtering algorithm is used in this paper to remove the noise. Fig. 7(c) shows the waveform of the picoelectric signal after removing the noise. Comparison of the amplitude, phase and spectral characteristics of the above waveforms verifies that the PEEK signal acquired by this system is accurate and valid.

6.4 Oxygen saturation data preprocessing and testing

On the basis of theoretical understanding of blood oxygen saturation and the acquisition approach of blood oxygen saturation mentioned above, both DC and AC components of the pulse waves will be extracted from the acquired data during the computation process; then, blood oxygen saturation will be computed following the computation theory mentioned in Section 2.3 of this paper. Since the existence of residual noise and artifacts in the extracted pulse waves may lead to errors in computing blood oxygen saturation, this system adopts the

filtering method proposed in Chapter 4 to eliminate the high frequency noise from the pulse wave data, and uses the fast median filter algorithm to remove the baseline drift in the data. Blood oxygen saturation results calculated through this system will be then compared with results of the same data collected by the MP150 system. The result comparison can be referred to in Table 4.

Table 4: Blood oxygen saturation test data

MP150 Measure blood oxygen saturation (times/points)	The system measures the oxygen saturation (sub-/ point)	Error(%)
80	81	1.25
82	82	0.00
84	85	1.19
86	87	1.16
88	89	1.14
90	91	1.11
92	93	1.09
94	95	1.06
96	96	0.00
98	99	1.02
100	101	1.00

6.5 Temperature Data Preprocessing and Testing

According to the previous description of the characteristics of body temperature and its acquisition method, the body temperature signal changes relatively slowly. The noise introduced by the circuit will cause the amplitude of the data read from the analog-to-digital converter to fluctuate greatly, which is contradictory to the slowly changing characteristics of the temperature. As such, the high frequency noises that are contained within the body temperature data are eliminated by this system by applying the sliding mean filtering technique, as explained earlier. In order to evaluate the accuracy of the body temperature measurements performed by this system, the measurements are validated against those performed using the MP150 system under identical circumstances. The findings of this comparison are shown in Table 5 and indicate that the difference between the two sets of measurements does not exceed 1.4%.

Table 5: Temperature data test control

MP150 Measured temperature(℃)	The temperature of the measurement of this system(℃)	Error(%)
36	36.4	1.11
36.2	36.2	0.00
36.4	36.7	0.82
36.6	36.6	0.00
36.8	37.1	0.82
37	37.3	0.81
37.2	37.6	1.08
37.4	37.7	0.80
37.6	38.1	1.33
37.8	38.3	1.32
38	38.3	0.79

7 Early Psychological Crisis Detection Experiment

7.1 Experimental program

Taking school graduate students as the experimental subjects, this paper designs the early psychological crisis state inducing experiment with psychological problems as the main factor, and carries out the collection of early psychological crisis state detection and identification data. The experiment takes measurements such as heart rate, blood pressure, blood oxygen saturation, and body temperature for subjects under two separate conditions: psychological health and psychological crisis, all while using a social media application actively. Following the previously mentioned advanced PSO-BP neural network model, early detection of psychological crisis is conducted for each subject and analyzed.

7.2 Physiological test data

A total of 300×4×2 data were collected in the two states, and Figs. 8-10 show the trends of the physiological parameters of the subjects in different states. Adolescent psychology when in a crisis state, the time for heart rate recovery is prolonged. Figure 8 depicts the fluctuations in heart rate between the two separate conditions. It is evident that heart rates measured during psychological crisis are significantly higher than those measured when the individual is psychologically healthy.

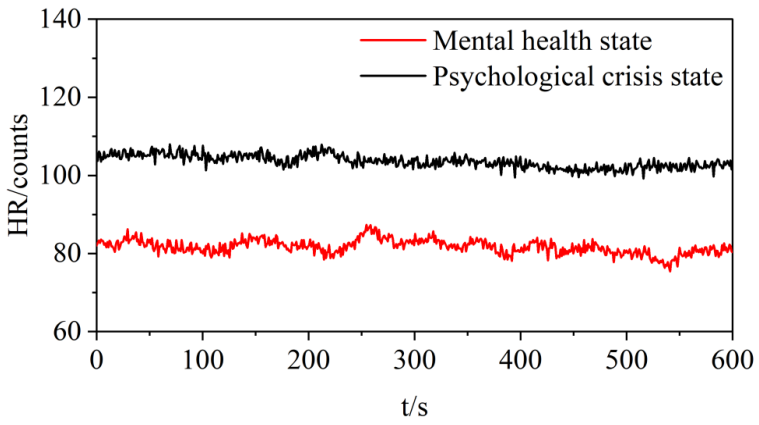

Figure 8: Heart rate change

Blood oxygen changes are shown in Figure 9, where the blood oxygen of the body fluctuates between 94% and 100% in the state of psychological health, which is a normal and safe level, and the value of blood oxygen saturation is lower in the state of psychological crisis. When the human body enters a state of psychological crisis, the responsiveness of the body's functions decreases, the inhaled oxygen decreases, and the oxygen level in the blood decreases, which further reduces the dynamics of the functions. When the concentration of oxygen in the blood decreases, blood circulation becomes slower and the body's oxygen supply decreases, which can exacerbate the response to the psychological crisis state.

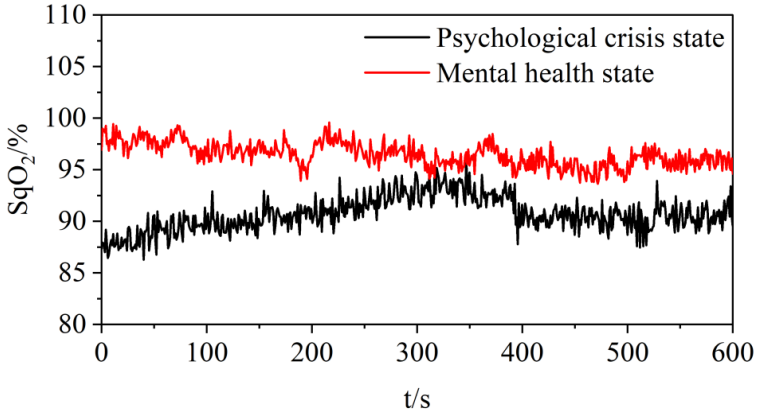

Figure 9: Blood oxygen changes

In order to facilitate the detection, the body temperature is selected from the temperature of the palm of the body surface, so the temperature value is slightly lower than the normal body temperature. Body temperature changes as shown in Figure 10, in the initial stage of measurement, the temperature sensor contact with the human body through heat conduction to achieve thermal equilibrium, so that it is consistent with the subject's body temperature, so the body temperature value in a short period of time to increase rapidly. The body temperature is in dynamic equilibrium in the state of mental health, while in the state of psychological crisis, the body temperature is lower than the temperature in the state of mental health.

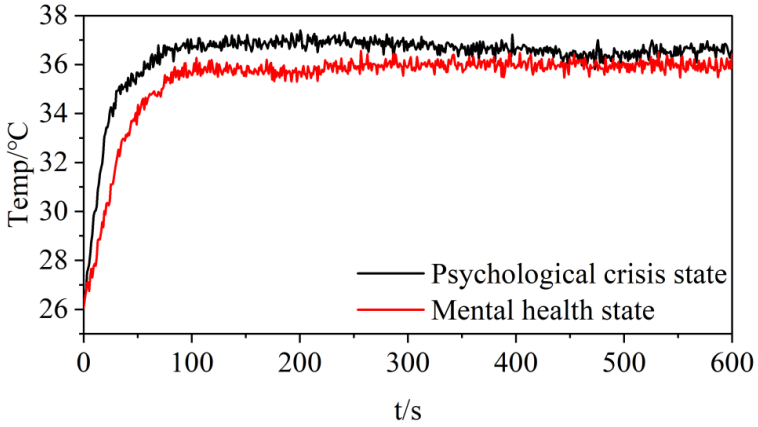

Figure 10: Temperature changes

7.3 Mental state identification results

(1) Analysis of training results

The experiment obtained a total of 800 sets of data, of which 400 sets are data in mental health state and 400 sets are data in psychological crisis state, and each set contains 5 dimensional features. All data samples were trained for test identification, of which 600 data were used as the training set, and the remaining 200 groups were used as the test set, with samples in the mental health state labeled 1, samples in the mild psychological crisis state labeled 2, and samples in the severe psychological crisis state labeled 3. During the training process, due to the varying orders of magnitude of the data, all the sample data were firstly normalized, so that the sample data are in the same order of magnitude, In turn, it helps improve the overall recognition accuracy of the model. Training parameters are given as follows: the maximum number of iterations is 2000; the target error is 0.001; the learning rate is 0.01. After

setting the basic parameters described above, the results of the prediction of final categories after training are shown in Figure 11.

The recognition model created through the use of the optimized PSO-BP neural network for training in the training set is then used to predict the category ranking of the test set samples. When comparing these results with the real labels of the test set, the final recognition accuracy turns out to be 95.5%, which means satisfactory recognition accuracy.

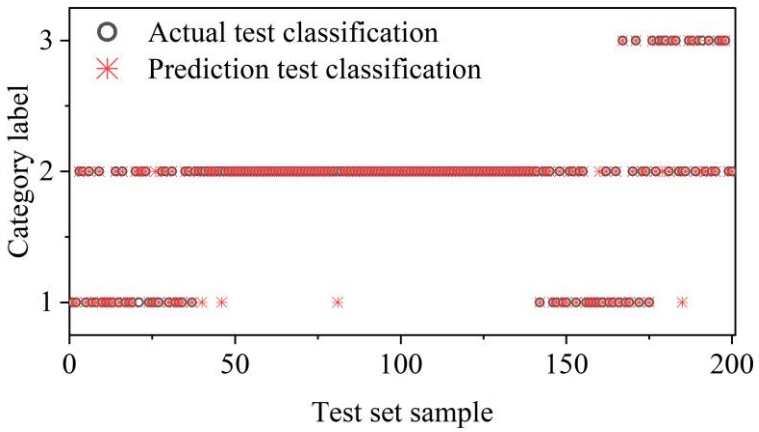

Figure 11: Actual identification and prediction recognition of the test set

With the help of such results, we receive the following results of the training by the mean square error and present them in Fig. 12. On the 40th iteration of our neural network, we receive the mean square error equal to 0.00027, which is lower than the specified target threshold. The difference between the two types of values shows the good accuracy of the recognition algorithm.

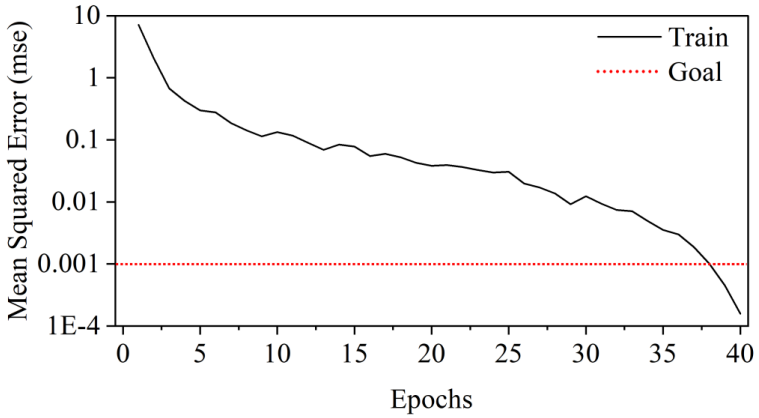

Figure 12: Error output results

In the early stage of data training, the random values for the weights and thresholds are set for the neural network. During training, however, they are continually updated based on the calculated error. By cycling back and forth, the network finally reaches its optimum point. In the current case, PSO is used to calculate the weights and thresholds of the neurons in the input layer and output layer. The results are shown in Tables 6 and 7.

Table 6: Neuron Weights and Thresholds in the Input Layer

Input layer	x_1	x_2	x_3	x_4	x_5	b_h
w_{i1}	-2.0000	1.9351	-1.8734	-1.2611	1.9056	-2.0000
w_{i2}	1.8497	-0.1976	2.0000	1.3640	1.9117	1.4001
w_{i3}	-0.6335	-2.0000	-0.0927	1.1721	0.4584	-1.9568
w_{i4}	2.0000	-1.5418	-1.0828	2.0000	-0.9527	1.1948
w_{i5}	-2.0000	-1.8612	2.0000	-1.2093	2.0000	-1.3836
w_{i6}	0.5482	2.0000	2.0000	2.0000	-1.9230	-2.0000
w_{i7}	-1.0771	-2.0000	1.9974	1.9637	1.9434	-1.8215
w_{i8}	-2.0000	-0.2637	-2.0000	-2.0000	-2.0000	2.0000
w_{i9}	-1.6317	-1.8542	-1.2736	1.9836	-1.9671	2.0000
w_{i10}	1.8846	-0.5318	0.1079	-1.8706	2.0000	-2.0000

Table 7: Output layer neuron weights and thresholds

Output layer	y_1	y_2	y_3
ω_{1o}	-1.8958	0.9976	-0.0264
ω_{2o}	1.8587	-1.6769	1.9009
ω_{3o}	1.7270	1.9783	0.0211
ω_{4o}	1.8575	0.8125	-2.0000
ω_{5o}	1.9474	-1.9321	1.3578
ω_{6o}	-2.0000	-1.8346	1.9394
ω_{7o}	-1.2037	-1.6079	1.9102
ω_{8o}	-1.8678	1.8313	1.5283
ω_{9o}	2.0000	2.0000	-1.9502
ω_{10o}	0.7728	-0.2950	2.0000
b_o	1.9627	-1.4275	1.9549

The threshold of a neuron denotes the amount of stimulation that the neuron needs in order to elicit a positive/negative excitation. In other words, with a higher threshold, more stimulation is needed before positive excitation occurs. When the input exceeds the threshold, it will cause the output to change, otherwise it will not have an effect on the output, optimizing the threshold can improve the BP neural network recognition rate. In BP neural network, by adjusting the weights to learn to get a nonlinear functional relationship that meets the requirements, the weight of each neuron is essentially the coefficient of each item, which indicates the degree of correlation between the input and the output, and therefore there are positive and negative. The weight denotes the contribution rate of an indicator to the output result and is shown in Table 8.

As shown above, regardless of the state, the greatest contribution rate among the indicators is achieved by the electroencephalogram signal, that is, the greatest degree of influence on the recognition results, followed by skin electricity, body temperature, blood oxygen, and the heart rate is relatively a little more influential role in the state of severe psychological crisis. In the mental health state, in which the influence weight of EEG reaches 0.2417, skin electricity 0.2048, and the greater influence is body temperature and blood oxygen, with weights of 0.2035,

0.2018. in the mild psychological crisis state identification, the influence weight of EEG is 0.2470, followed by skin electricity, blood oxygen, and body temperature, with weights of 0.2014, 0.2200, respectively, 0.2160.In the category of severe psychological crisis state, the influence weights of EEG and ECG amounted to 0.2704 and 0.2550, followed by body temperature with a weight of 0.1805.

Table 8: Contribution Rate and Weight of Physiological Parameters to Output State

Physiological parameters		Heart rate	Blood oxygen	Body temperature	Pigmentation	Brain electricity
Mental health	Contribution rate	5.2716	7.1852	7.2460	7.2905	8.6054
	Weighting	0.1481	0.2018	0.2035	0.2048	0.2417
Mild psychological crisis	Contribution rate	7.2160	13.7498	13.4967	12.5863	15.4364
	Weighting	0.1155	0.2200	0.2160	0.2014	0.2470
Severe psychological crisis	Contribution rate	5.2075	3.9729	5.6336	7.9584	8.4394
	Weighting	0.1668	0.1273	0.1805	0.2550	0.2704

(2) Recognition results analysis

After the BP neural network to get 800 recognition results, due to the collection of physiological data process, the temperature sensor needs to be heat conduction to achieve consistent with the human body temperature, so the unified removal of the first 2 minutes of data, retaining the stable data within 2 ~ 10 minutes, recognition details shown in Figure 13.

The physiological parameters collected in the mental health state are all in category 1, i.e., the mental health state. The physiological parameters collected in the psychological crisis state were more distributed in categories 2 and 3, i.e., mild psychological crisis and severe psychological crisis. The physiological indicators under severe psychological crisis were mainly concentrated in 3~6 minutes after the start of data collection. In 6~7 minutes and the last minute of the test, due to the fluctuation of physiological parameters few physiological indicators were classified into the safe category. The physiological parameters collected in this psychological crisis state inducing experiment were mainly distributed in the mild psychological crisis category.

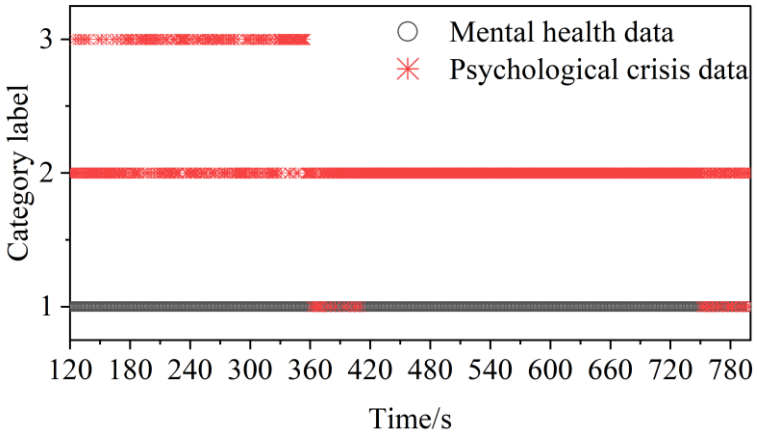

Figure 13: Results of identifying psychological crisis states

8 Mental Health Early Warning System Construction

The physiological signal analysis and psychological warning system designed in this paper requires deep learning, but due to reasons such as fewer dataset samples and the fact that changes within dataset classes can affect the deep learning network, to overcome the limitations pointed out in the above section, some necessary improvements should be made to the PSO-BP neural network algorithm in terms of constructing a physiological data analysis and psychological early warning system.

As for the process to carry out when training with the enhanced PSO-BP neural network algorithm, the following is the particular implementation procedure. First, select the facial data set and optimize its weights in such a way that the absolute value of its weight will not exceed the range around zero. Secondly, filter the photos in the training sample set. Thirdly, compute the difference between the target output and the real output vectors so that to obtain the error between them. Fourthly, compute the error of each hidden layer neuron. Fifthly, define the range of variation for the weights and thresholds. Sixthly, adjust both the weights and the thresholds before checking whether the achieved accuracy meets the requirements defined in the constraints. Seventhly, apply the enhanced PSO algorithm to update the weight coefficients across the neural network. When the required training accuracy is reached, the thresholds and weights of the BP neural network are retained; thus, the training process for the enhanced PSO-BP neural network algorithm ends.

Variations in the environment of capturing the feedback images by the physiological signal analysis and psychological early warning system constructed on the basis of the enhanced PSO-BP neural network cause intraclass variations, and intraclass differences will seriously affect the training results of the neural network, therefore, in order to ensure that the improved PSO-BP neural network in the application of the process of better robustness, so as to obtain accurate training results, it is necessary to select a multi-source database, and then the BP neural network can be used for training. It is necessary to select the multi-source database. The inclusion of samples in the multivariate database to be used in the training process of the optimized PSO-BP algorithm greatly increases the variation in the facial image samples, reducing the correlation between action units, the intensity of action units, and training samples. Additionally, the thoughtful selection of sample data ensures the elimination of any subjective factors in the process of selecting samples.

With the help of a neural network database being built according to the improved PSO-BP neural network in terms of physiological signal analysis and psychological early warning system, this kind of system will no longer rely on the usual Windows operating system but instead use the Robot Operating System (ROS). Such system provides the basic framework for its operation. In order to collect facial data, a camera will need to be installed for the monitoring of such subjects; thus, the selected equipment would be Kinect 2.0 RGBD camera, which possesses these characteristics: an RGB resolution of 1024x768, a depth resolution of 512x424, detection range ranging from 0.5meters to 5 meters, and detection angle of 85 degrees. With the establishment of the psychological early warning system, whenever there is an unusual change in the psychological conditions of the monitored subject, then a complete analysis will be carried out. The system will refer to psychological case data to understand the issue, and send out an early warning through UDP communication protocol to the electronic terminal of the subject concerned along with relevant assisting data.

9 Conclusion

In this paper, the psychological state of adolescents expressed during the process of socializing online is analyzed by means of multimodal data using an improved PSO-BP algorithm with the purpose of developing a psychological early warning system that can accurately detect early psychological crises in adolescents.

In this paper, the cardiac, cerebral, oxygen saturation, picoelectric, and body temperature data of adolescents in the online socialization state are collected by the designed multimodal data acquisition system. Comparing the physiological signals collected by the MP150 system, the signals collected by this system are basically the same in terms of amplitude, phase and spectral characteristics of the waveforms, and none of them has an error of more than 2%. The PSO-BP algorithm proposed in this paper is able to effectively identify and classify psychological states using physiological features with an average accuracy rate of 95.5% and a lowest error value of 0.00027. After finding the weights and thresholds of the physiological feature indicators using the proposed PSO-BP algorithm, the influence weights of the EEG indicators are the largest in all three states of mental health, mild psychological crisis, and severe psychological crisis.

Funding

This work was supported by the President's Fund of Tarim University - Hu Yang Talent Introduction Research Start-up Fund (Doctoral Program) (Project: Construction of Intelligent Screening Model for College Students' Psychological Crisis: A Case Study of Tarim University; Grant No. TDSKBS202506).

About the Author

Hui Xu was born in Shenqiu County, Henan Province, China, in 1985. He holds a Doctor of Education (Ed.D.) degree and is currently a faculty member at the Student Affairs Office of the University Party Committee, Tarim University. His research focuses on mental health education, crisis identification, and intervention.

Huazhi Li was born in 2003 in Pingyuan County, Dezhou City, Shandong Province, China. He obtained his bachelor's degree from Xinxiang University and is currently pursuing a graduate degree at the School of Computer Science and Technology, Xinjiang University. His research areas include big data analysis and intelligent

Huanhuan Luo was born in 1985 in Fugou County, Henan Province, China. She earned her Doctor of Philosophy (Ph.D.) in Medical Science from Huazhong University of Science and Technology. She is currently affiliated with the School of Medicine at Tarim University, specializing in the research fields of Basic Medicine and Medical Psychology.

References

[1] Bessarab, A., Mitchuk, O., Baranetska, A., Kodatska, N., Kvasnytsia, O., & Mykytiv, G. (2021). Social networks as a phenomenon of the information society. Journal of Optimization in Industrial Engineering, 14(Special Issue), 17-24.

[2] Carr, C. T., & Hayes, R. A. (2015). Social media: Defining, developing, and divining. Atlantic journal of communication, 23(1), 46-65.

[3] Sadiku, M., Omotoso, A. A., & Musa, S. (2019). Social networking. International Journal of Trend in Scientific Research and Development, 3(3), 126-128.

[4] Saleh, E. F. (2024). Adolescent Socialization in the Digital Age: The Role of Internet Usage and Social Networks. Recent Research Advances in Arts and Social Studies, 66-98.

[5] Wu, Y. J., Outley, C., Matarrita-Cascante, D., & Murphrey, T. P. (2016). A systematic review of recent research on adolescent social connectedness and mental health with internet technology use. Adolescent Research Review, 1(2), 153-162.

[6] Kerr, S., & Kingsbury, M. (2023). Online digital media use and adolescent mental health. Health reports, 34(2), 17-28.

[7] Buonomo, I., Cipriani, I., Piperno, S., Saddi, I., & Fiorilli, C. (2015). Internet and Socialization How Internet use influences online and offline relationships. Anthropological Researches and studies, 1(5), 3-10.

[8] Benrouba, F., & Boudour, R. (2023). Emotional sentiment analysis of social media content for mental health safety. Social Network Analysis and Mining, 13(1), 17.

[9] Aksoy, S. (2025). Textual Sentiment Analysis for Mental Health Diagnosis. In Adversarial Deep Generative Techniques for Early Diagnosis of Neurological Conditions and Mental Health Practises: Theoretical Insights with Practical Applications (pp. 301-321). Cham: Springer Nature Switzerland.

[10] Gaw, N., Yousefi, S., & Gahrooei, M. R. (2022). Multimodal data fusion for systems improvement: A review. Handbook of Scholarly Publications from the Air Force Institute of Technology (AFIT), Volume 1, 2000-2020, 101-136.

[11] Pawłowski, M., Wróblewska, A., & Sysko-Romańczuk, S. (2023). Effective techniques for multimodal data fusion: A comparative analysis. Sensors, 23(5), 2381.

[12] Tian, X., Zheng, Q., & Jiang, N. (2021). An Abnormal Behavior Detection Method Leveraging Multi-modal Data Fusion and Deep Mining. IAENG International Journal of Applied Mathematics, 51(1).

[13] Zhang, H., Cao, L., Feng, L., & Yang, M. (2020). Multi-modal interactive fusion method for detecting teenagers' psychological stress. Journal of Biomedical Informatics, 106, 103427.

[14] Song, B., Liu, P., & Chen, X. (2025). AWNB: Augmented-Wingsuit–Optimized Multinomial Naïve Bayes for Multimodal Early-Warning of College Student Mental Health. Informatica, 49(36).

[15] Liu, C., & Lei, Y. (2024, July). The Application of Artificial Intelligence Technology in School Psychological Crisis Warning Work. In Proceedings of the 2nd International Conference on Educational Knowledge and Informatization (pp. 526-530).

[16] Wu, Y. (2025). Data Fusion Model for Psychological Crisis Early Warning System Using Data Mining Techniques. Informatica, 49(23).

[17] Zhang, X. (2023). The impact of online socialization on adolescent mental health: The mediating role of friendship quality and family relationships. New Directions for Child and Adolescent Development, 2023(1), 7007025.

[18] Pantic, I. (2014). Online social networking and mental health. Cyberpsychology, Behavior, and Social Networking, 17(10), 652-657.

[19] Law, D. M., Shapka, J. D., & Collie, R. J. (2020). Who might flourish and who might languish? Adolescent social and mental health profiles and their online experiences and behaviors. Human Behavior and Emerging Technologies, 2(1), 82-92.

[20] Birgisson, O., Hysing, M., Eriksen, H. R., Johannsson, E., & Gestsdottir, S. (2024). The relationship between online communication and adolescents' mental health: Long-term evaluation between genders. Scandinavian journal of public health, 52(4), 486-493.

[21] Pachucki, M. C., Ozer, E. J., Barrat, A., & Cattuto, C. (2015). Mental health and social networks in early adolescence: A dynamic study of objectively-measured social interaction behaviors. Social science & medicine, 125, 40-50.

[22] Prochnow, T., Senthil, R., Poulos, A., Patterson, M. S., Blake, J., & Massey, P. (2025). Virtual Bonds; Real Emotions: Systematic Review Exploring Online Social Connections and Adolescent Mental Health. Cyberpsychology, Behavior, and Social Networking, 28(10), 658-671.

[23] Odgers, C. L., & Jensen, M. R. (2020). Annual research review: Adolescent mental health in the digital age: Facts, fears, and future directions. Journal of Child Psychology and Psychiatry, 61(3), 336-348.

[24] Sembiring, T. B., & Mokodenseho, S. (2023). The Impact of Online Interactions on Mental Health among Adolescents in West Java. The Eastasouth Journal of Social Science and Humanities, 1(01), 1-9.

[25] Best, P., Manktelow, R., & Taylor, B. (2014). Online communication, social media and adolescent wellbeing: A systematic narrative review. Children and Youth Services Review, 41, 27-36.

[26] Pontes, H. M. (2017). Investigating the differential effects of social networking site addiction and Internet gaming disorder on psychological health. Journal of behavioral addictions, 6(4), 601-610.

[27] Abi-Jaoude, E., Naylor, K. T., & Pignatiello, A. (2020). Smartphones, social media use and youth mental health. Cmaj, 192(6), E136-E141.

[28] Flynn, H. C., Mote, S. L., & Morse, B. L. (2022). Social media and adolescent mental health: sounding the alarm. NASN school nurse, 37(5), 271-276.